



Seismic amplification factor and dynamic response of soil-nailed walls

Mahdi Maleki¹ · Ali Khezri¹ · Masoud Nosrati² · Seyed Majdeddin Mir Mohammad Hosseini¹

Received: 2 July 2022 / Accepted: 22 September 2022 / Published online: 12 October 2022
© The Author(s), under exclusive licence to Springer Nature Switzerland AG 2022

Abstract

The satisfactory performance of the soil-nailed walls during strong ground motions and their superior flexibility compared to the other guard structures makes them a preferable stabilizing alternative when the risk of seismic loading prevails. The dynamic performance of a deep excavation during a seismic event is greatly influenced by the characteristics of the input motion (fundamental frequency, amplitude, and duration) as well as the properties of geo-materials. Site effect is yet another factor capable of altering the dynamic response of such structures. It has been proven that such site effects as amplification factor and topography effect can be quite influential in the overall seismic performance of earth structure. The present study investigates the effects of mechanical (nails' axial stiffness and soil–nail interface friction coefficient) and geometrical (angle, length, vertical and horizontal spacing) properties of the nails on the dynamic response and the amplification characteristics of a retained trench wall in both loose and dense soil conditions. It was found that the factors leading to the increase in the stability of the reinforced wall would also lead to the increase in the wall's amplification factor. Moreover, the greatest amplification factor has been computed in the immediate vicinity of the wall, and the factor decreases by moving farther away from the wall, converging to that of the free-field condition. It was also noted that the vertical spacing of the nails is more influential in the control of the settlement of the adjacent ground compared to the horizontal spacing.

Keywords Soil-nailed walls · Finite element method · Safety factor · Amplification · Seismic response

Introduction

Its flexibility with regard to the construction conditions, cost-effectiveness, convenient implementation, and satisfactory performance have made the soil nailing technique a popular and common earth retention method. The technique has been first introduced in the 1970s and since then has been widely used to retain natural or man-made excavations under static or dynamic loading conditions. Previous

post-earthquake observations have testified to the excellent performance of the soil-nailed wall systems during sturdy ground motions (Colin et al. 1992; Tatsuoka et al. 1995). For instance, during the 1989 Loma Prieta earthquake, nailed excavations in the vicinity of the earthquake epicenter functioned remarkably well under intense ground shakings. Other examples of exceptionally well performance of soil-nailed wall systems (e.g., 1995 Kobe earthquake and 2001 Nisqually earthquakes) can confirm their intrinsically remarkable dynamic response, which mainly stems from their high levels of flexibility—and to some extent from the conservative assumptions in their design (Yazdandoust 2017).

Typically, seismic considerations are not accounted for in the design of temporary excavations, yet when dealing with the design of permanent excavations or stabilization of steep slopes, seismic considerations should be taken into account—especially in earthquake-active areas. Pseudo-static and dynamic analyses are often carried out in the stability assessment of stabilized trench walls. The pseudo-static method is performed by considering the horizontal and vertical forces induced by earthquake vibrations in the center of the slope's failure wedge (Kramer 1996). The

✉ Mahdi Maleki
mahdi1793@aut.ac.ir

Ali Khezri
Ali94kzr@aut.ac.ir

Masoud Nosrati
m.nosrati5979@gmail.com

Seyed Majdeddin Mir Mohammad Hosseini
Smmirhos@aut.ac.ir

¹ Department of Civil and Environmental Engineering, Amirkabir University of Technology, Tehran, Iran

² Department of Civil and Environmental Engineering, Tarbiat Modares University, Tehran, Iran

pseudo-static analysis method, unlike the dynamic method, is unable to capture the cyclic and time-dependent nature of actual seismic forces.

In recent years, the stability of trench walls reinforced by nails has been investigated using such methods as the limit equilibrium method (LEM) (Wei et al. 2010; Rawat and Gupta 2016; Deng et al. 2017), the limit analysis method (LAM) (Michalowski and You 2000; Giri and Sengupta 2009; He et al. 2012), and the finite element method (FEM) (Bang and Chung 1999; Sivakumar Babu and Murthy 2002; Siva Kumar Babu et al. 2008; Fan and Luo 2008; Wu and Shi 2010; Jaya and Annie 2013; Johari et al. 2020), among which, the finite element method, capable of clearly revealing the stress–strain relationship of nail-reinforced slopes, is becoming standard practice in analyzing the stability of slopes (Sahoo et al. 2015; Chavan et al. 2017; Farrokhzad et al. 2017).

A fair few research studies have investigated the performance of deep excavations under seismic loading in the last decades. Mark and Mladen (2000) performed a series of dynamic centrifuge tests to investigate the kinematics and failure mechanism of four soil-nailed excavation models under horizontal cyclic loading. They reported that large amplitudes of horizontal accelerations were needed to start off substantial displacements in the modeled soil-nailed wall, implying that prototype soil-nailed systems should be quite stable during intense seismic shakes. Chavan et al. (2017) have investigated the seismic behavior of typical nailed slopes by taking into account the soil nonlinearity and pressure dependency using a two-dimensional finite element model based on the OpenSees platform. They concluded that the modeling of the soil–nail interface could substantially influence the slopes' permanent deformations after earthquake loading. They also showed that the overburden pressure on the nail varies considerably during seismic loading, especially when sliding and separation occur at the soil–nail interface.

The effect of loading duration, peak acceleration, and nails' length on the seismic performance of soil-nailed walls with regard to the distribution of the shear modulus and damping ratio in the soil mass has been investigated by Yazdandoust in a series of 1 g, shaking table tests (Yazdandoust 2017). He pointed out that the seismic response of the walls is largely dependent on the nails' length and input motion parameters. Yang et al. (2020) assessed the stability of nail-reinforced slopes using the three-dimensional rotational failure mechanism based on the strength reduction method (SRM) in combination with the kinematic approach of the limit analysis. The influence of such parameters as nails' length and spacing, as well as the soil shear strength, on the stability of slopes has been evaluated. They finally presented a set of stability charts for a quick assessment of slope stability.

Babu et al. (2008) studied the seismic performance of a typical soil-nailed wall system, designed in accordance with the FHWA design procedure, through numerical simulation. They concluded that the pseudo-static analyses yield conservative results for displacements and safety factor values as compared to those acquired from the time histories of the considered earthquake vibrations. Debabrata and Aniruddha (2010) conducted a series of laboratory shaking table tests and numerical simulations to study the dynamic behavior of steep slopes reinforced by nails. Their results indicated that the induced nail forces vary nonlinearly with respect to loading cycles. They also found out that, due to the inadequate soil confining pressure, the top row nails did not generate considerable force as compared to the other (lower) rows. Moniuddin et al. (2016) studied the performance of a nail-stabilized excavation under static and seismic conditions using a numerical model. They also confirmed the satisfactory seismic response of nail-stabilized trenches.

Tavakoli et al. (2019) studied the effect of embedded length of the sheet piles, underground water table, and shear wave velocity of soil on the amplification factor of a trench wall stabilized by a nailing system. They reported that the amplification factor increases as the embedment depth of the sheet piles and the length of the nails increase.

Sharma et al. (2020) investigated the performance of helical soil-nailed walls under static and seismic conditions through a detailed parametric study in which the effect of angle of internal friction of soil, nails' inclination angle and vertical spacing, helix size, number of helices, and the face angle on the stability of the wall have been evaluated. The results obtained emphasized the importance of input excitation frequency on the safety factor of helical soil-nailed walls.

Chatterjee (2022) studied the effect of surcharge loading on the seismic performance slopes reinforced by nails. They proposed close form expressions for obtaining the equivalent pullout capacity of the nails and safety factor considering the influence of surcharge load, seismic forces, angle of the failure plane, slope angle, nails inclination angle, and nails spacing. They reported that the increase in the nails' inclination angle increases the equivalent pullout capacity of the nails as well as the failure angle of the wedge. They also showed that the increase in the nails' horizontal spacing decreases the equivalent pullout capacity of the nails and the angle of the failure wedge.

Chen et al. (2022) introduced a modified pseudo-dynamic approach capable of incorporating the impact of earthquake loads into the slope stability analysis of slopes reinforced by inclined nails. They showed that the ratios of seismic acceleration (for the slope crest to the slope toe) greatly influence the slope stability under seismic actions. They also reported that under a specific nail inclination angle, the best performance for the reinforcement could be achieved.

Despite a significant amount of research conducted on the stability of nailed slopes and excavations under static and dynamic loading conditions, their dynamic response considering the influence of such site effects as soil amplification and topography effect has remained relatively unexplored in the literature, although they are expected to have a substantial impact on the overall performance of the nailed trench walls. This is addressed herein, numerically through a two-dimensional finite element analysis using equivalent linear behavior. The developed models have been used to investigate the effect of different mechanical and geometrical properties of the nails on the stability and deformation of the trench wall, the settlement of the adjacent ground, and the amplification factor of different locations on the model. The parameters investigated include the nails' inclination angle, length, axial stiffness (EA), horizontal and vertical spacing, as well as soil–nail friction coefficient. The above-mentioned responses have been studied in both loose and dense sites at different locations on the wall and the adjacent ground.

Numerical modeling

In the present research, a series of seismic analyses have been performed based on a two-dimensional, plain-strain model developed using the Plaxis software. The numerical model is originally based on a man-made trench wall in downtown Tehran, Iran's capital city. The city is located in a seismically active region on an alluvial plain immediately south of Alborz Mountains Range. The alluvial plain, composed of Quaternary gravels, sands, silts, and boulder beds, is formed by flood erosion of the mountains. This process resulted in the settlement of large and small particles on high and low elevations, respectively, resulting in heterogeneous geological conditions (Knill and Jones 1968; Fagher et al. 2007). The geometry of the excavation (including its reinforcements) and the adjacent building is illustrated in Fig. 1.

Fig. 1 Schematic of the model used in the present study

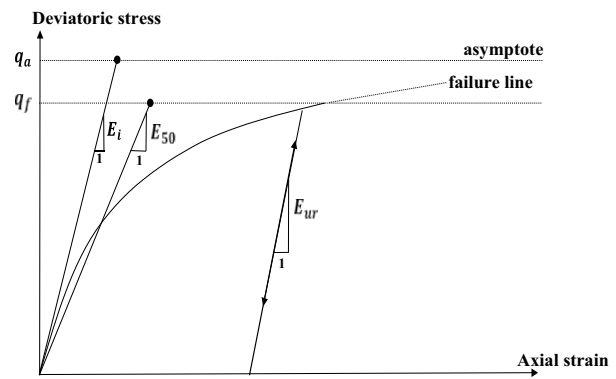
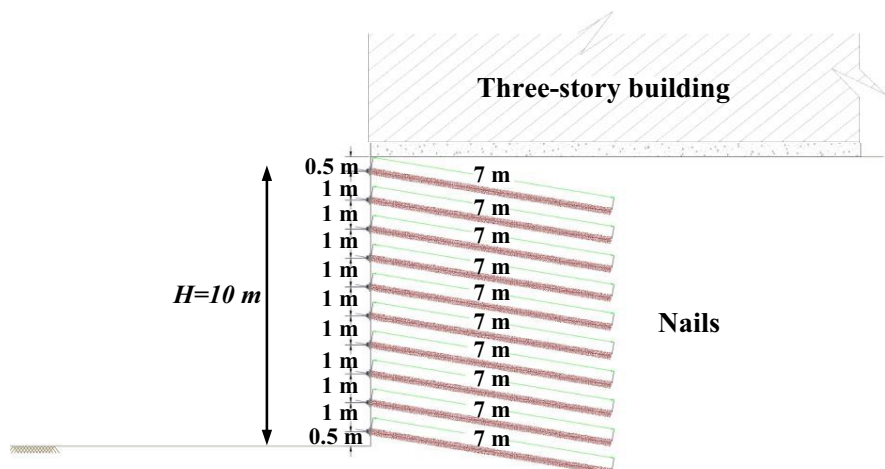


Fig. 2 The hyperbolic stress–strain curve used in the Hardening soil model (Duncan and Chang 1970)

Varying soil density conditions have been considered for the model. As no groundwater table has been witnessed during the excavation, no water table has been considered for the model. A three-story building in the immediate vicinity of the trench wall was also modeled.

The soil layer was modeled using 15-node triangular elements. For the structural components (i.e., the nails and the facing of the soil-nailed wall), nonvolume plate elements were used. In what follows, a description of the soil model, structural elements, boundary conditions, interface elements, and the created finite element mesh will be presented in detail.

The hardening soil model (HS), an advanced model for the simulation of different types of soils, is employed in the modeling of the soil medium in this study (Schanz et al. 1999). The major advantage of this behavioral model compared to others (e.g., the Mohr–Coulomb model) is its ability to take into account the stress dependency of the soil stiffness, enabling it to accurately model the stiffness and deformation behavior before the material failure. As shown in Fig. 2, the HS model proposed by Duncan and

Chang (1970) adopts a hyperbolic stress–strain relation between the vertical strain (ε_1) and deviatoric stress (q) for the primary loading. The hardening soil behavioral model uses three different input stiffness parameters, namely; triaxial loading secant stiffness E_{50}^{ref} , triaxial unloading/reloading stiffness $E_{\text{ur}}^{\text{ref}}$, and oedometer loading tangent stiffness $E_{\text{oad}}^{\text{ref}}$ at a reference pressure (p^{ref} , usually taken as 100 kPa); to calculate soil stiffness (Peng et al. 2011). Other input parameters of HSM include cohesion (c (kN/m²)), friction angle (φ (°)), dilatancy angle (ψ (°)), and Poisson's ratio (ν). The coefficient of lateral earth pressure at rest (K_0) can be determined by Eq. (1) (Jaky 1994):

$$K_0 = 1 - \sin \varphi. \quad (1)$$

The dilation angle (ψ) of the cohesionless materials depends on their relative density and friction angle. For soil aggregates with an internal friction angle greater than 30°, the dilation angle is estimated at about $\psi = \varphi - 30^\circ$ (Bolton 1986), and for soil aggregates with an internal friction angle less than 30°, the dilatation angle is $\psi = 0^\circ$. The failure ratio (R_f) is considered 0.9 as a default value in the Plaxis software (reference manual of the Plaxis software 2017). The friction angle (φ) for the sand layer was directly obtained from laboratory tests. Values of cohesion (c) for soil layers were assumed to be zero, but to avoid complications in software calculations, a very small value of $c = 0.5$ kPa was set for the soil layers. According to the suggestion of Khoiri and Ou (2013), the drained Poisson ratio was assumed to be 0.3 for the soil layers.

In the dynamic analyses, based on the type of analysis (nonlinear or linear equivalent), behavioral models capable of considering such parameters as shear modulus, shear strain, and damping coefficient should be used. Among different behavioral models defined in Plaxis software, Hardening soil with small strain (HS-Small) is the only behavioral model capable of considering such parameters, making it a perfect fit for modeling dynamic problems. In other words, alternative behavioral models fail to consider damping before reaching plastic behavior as shear modulus and damping are not a model input in them. In the alternative behavioral models, it is essential to determine material damping. To this end, Rayleigh damping (Clough and Penzien 1993) is applied to materials in which damping matrix (C) is associated with the components of stiffness (K) and mass (M) matrixes, using α and β factors, as shown in Eq. (2).

$$C = \alpha M + \beta K. \quad (2)$$

The α factor denotes the damping coefficient related to mass, and β stands for the damping coefficient connected to stiffness, and it can be calculated using Eq. (3) as follows:

$$\alpha + \beta \omega_i^2 = 2\omega_i \xi_i, \quad (3)$$

where ξ_i is the critical damping ratio, which is 0.05 for all materials, and ω_i is the angular frequency in two vibration modes.

Plotting soil stiffness against strain (log) yields a characteristic s-shaped stiffness-reduction curve, as shown in Fig. 3. Brinkgreve et al. (2012) deduced that the strain range in which soils can be considered truly elastic is very small, and as the strain amplitude increases, soil stiffness decays nonlinearly (Atkinson and Salfors 1991). The soil stiffness used in the analysis of geotechnical structures should consider the very small-strain stiffness and its nonlinear dependency on strain amplitude. Therefore, the Hardening Soil with small strain behavioral model (HS-Small) was implemented for material modeling in the present study.

The HS-Small model includes all of the input parameters in the HS behavioral model in addition to three extra material parameters, which are needed to be described to consider the variations in stiffness based on strain. These additional parameters are the initial or very-small-strain shear modulus G_0 , reference shear modulus (G_0^{ref}) at very small strains, and the shear strain ($\gamma_{0.7}$), at which $G_s = 0.722G_0$. The shear modulus in small strains (G_0) can be determined either through field and laboratory tests (Atkinson and Salfors 1991; Viggiani and Atkinson 1995; Rampello et al. 1997; Kurtulus and Stokoe 2008) or using theoretical equations. In the present study, the shear modulus G_0 is calculated from Eq. (4) (Brinkgreve et al. 2012):

$$G_0 = G_0^{\text{ref}} \left(\frac{c \cos \varphi - \sigma'_3 \sin \varphi}{c \cos \varphi + P^{\text{ref}} \sin \varphi} \right)^m. \quad (4)$$

The reference shear modulus G_0^{ref} at very small strains ($\varepsilon < 10^{-6}$) for $p^{\text{ref}} = 100$ kPa can be estimated from Eq. (5) (Benz 2007):

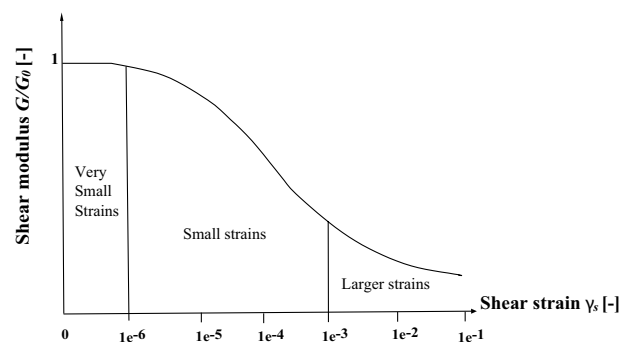


Fig. 3 Characteristic stiffness-strain behavior in logarithmic scale (Atkinson and Salfors 1991)

$$G_0^{ref} = 33 \times \frac{(2.97 - e)^2}{1 + e} \text{ (MPa)}. \tag{5}$$

The parameter $\gamma_{0.7}$ can be calculated using Eq. (6) (Peng et al. 2011):

$$\gamma_{0.7} \approx \frac{1}{9G_0} [2c'(1 + \cos(2\phi')) - \sigma'_1(1 + K_0) \sin(2\phi')]. \tag{6}$$

In the above equations, m = power for stress-level dependency of stiffness ($m=0.5$ for dense soil and $m=1$ for loose soil); e = initial soil void ratio (-); E_{50}^{ref} = secant stiffness in the standard drained triaxial test (kN/m²); E_{oed}^{ref} = tangent stiffness for primary oedometer loading (kN/m²); E_{ur}^{ref} = unloading/reloading stiffness at engineering strains (kN/m²); ν_{ur} = Poisson’s ratio for unloading/reloading ($\nu_{ur}=0.3$ in this study); G_0^{ref} = reference shear modulus at very small strains (kN/m²); $\gamma_{0.7}$ = shear strain at which $G_s=0.722G_0$; K_0 = earth pressure coefficient at rest; σ'_1 = vertical principal effective stress (pressure negative) (kN/m²); and σ'_3 = horizontal principal effective stress (pressure negative) (kN/m²). The values considered for HS-Small model parameters of sand layers are given in Table 1.

The design of the soil-nailed wall is carried out in accordance with the allowable stress design procedure of the FHWA code. A shotcrete coating with a thickness of 20 cm was simulated by plate elements as the facing of the soil-nailed wall. The facing, which is supported by the nail system, can bear both horizontal forces and bending moments. The nails were simulated with geogrid elements, only able to bear tensile forces. The nails’ axial stiffness is determined by $E_{eq}A$, where E_{eq} is the equivalent modulus of elasticity for the grouted soil nails, and A is the total cross-sectional area of the grouted soil nails. The soil-nailed wall system is generally 3D. For modeling grouted nails in 2D plane strain analysis, the use of equivalent nail parameters is necessary. The equivalent modulus of elasticity E_{eq} is expressed using Eq. (7) as follows (Singh and Sivakumar Babu 2010):

$$E_{eq} = E_n \left(\frac{A_n}{A} \right) + E_g \left(\frac{A_g}{A} \right), \tag{7}$$

where E_n is Young’s modulus of nails, which was taken to be 2×10^5 (MPa), A_n is the cross-sectional area of a reinforcement bar, A is the total cross-sectional area of the grouted soil nail, E_g is Young’s modulus of grout material, and A_g is the cross-sectional area of grout cover. The parameters A , A_n , and A_g can be calculated using Eqs. (8) to (10), respectively.

$$A = \frac{\pi D_{DH}^2}{4}, \tag{8}$$

$$A_n = \frac{\pi d^2}{4}, \tag{9}$$

$$A_g = A - A_n, \tag{10}$$

D_{DH} is the diameter of the drilled hole in the above-mentioned equation. By knowing the E_{eq} for the grouted soil–nail and the horizontal spacing of the nails (S_h), the axial stiffness can be calculated using Eq. (11):

$$EA = \frac{E_{eq}}{S_h} \left(\frac{\pi D_{DH}^2}{4} \right). \tag{11}$$

For both the concrete facing and nails, the linear elastic model has been used. The modulus of elasticity of the concrete facing has been calculated using Eq. (12) (ACI Committee 318 1995):

$$E_c = 4700 \sqrt{f'_c}, \tag{12}$$

where f'_c is the standard compressive strength of the concrete facing.

The parameters of the modeled concrete facing and the nails are given in Tables 2 and 3, respectively.

Table 1 Soil parameters used in the finite element analysis

Parameter	Dense soil	Loose soil
Soil type	SM	SM
Soil unit weight, γ (kN/m ³)	19.5	19
Cohesion, c (kN/m ²)	0.5	0.1
Internal friction angle, ϕ (degree)	34°	24.5°
Dilatancy angle, ψ (degree)	4°	0°
Poisson’s ratio, ν	0.3	0.3
Reference secant stiffness from the drained triaxial test, E_{50}^{ref} (kN/m ²)	8.325×10^4	2×10^4
Reference tangent stiffness for oedometer primary loading, E_{oed}^{ref} (kN/m ²)	8.325×10^4	2×10^4
Reference unloading/reloading stiffness, E_{ur}^{ref} (kN/m ²)	2.498×10^5	6×10^4
Exponential power, m	0.5	1

Table 2 Shotcrete facing parameters used in the finite element analysis

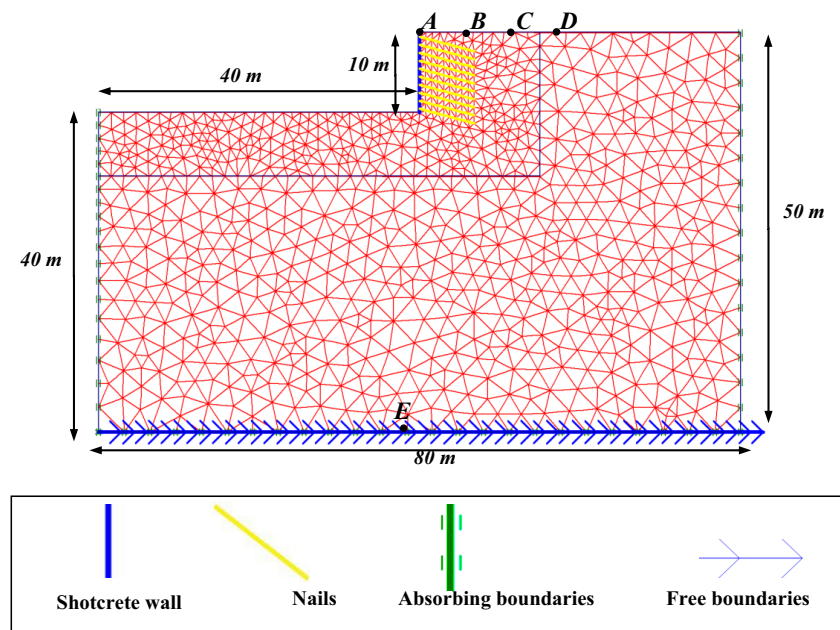
Parameter	Value
Unit weight, γ (kN/m ³)	24
Poisson's ratio, ν	0.2
Young's modulus, E_c (kN/m ²)	22×10^6
Compressive strength of concrete, f'_c (MPa)	21.9
Normal stiffness of shotcrete coated wall, EA (kN)	4.4×10^6
Flexural rigidity of shotcrete coated wall, EI (kN m ²)	1.47×10^4
Vertical height of the wall, H (m)	10
Facing thickness, t (cm)	20
Slope of backfill, β (degree)	0°
Face batter, α (degree)	0°

Table 3 Nail parameters used in the finite element analysis

Parameter	Value
Nail spacing, $S_v \times S_h$ (m \times m)	1.0×1.0
Nail inclination (with horizontal), i (degree)	15°
Length of nails, L (m)	7
Diameter of nails, d (mm)	20
Yield strength of nail, f_y (MPa)	415
Drill hole diameter, D_{DH} (mm)	100
Modulus of elasticity of nail, E_n (GPa)	200
Modulus of elasticity of grout (concrete), E_g (GPa)	20
Normal stiffness of nails, $E_{eq}A$ (kN)	2.136×10^5
Poisson's ratio, ν	0.2

The geometry of the finite element model, along with its specifications, is presented in Fig. 4. The distance of the excavation from the boundaries was selected such that their effect on the results would be minimized (Lees 2007). Furthermore, the model's left and right boundaries were fixed only in the horizontal direction, while the base of the models was fixed in both the horizontal and vertical directions (Fig. 4). After creating static boundary conditions, dynamic boundary conditions were created in the model. To avoid the reflection of the earthquake waves when they strike side boundaries, absorbing boundaries have been assigned to the model's sides. On the other hand, a standard earthquake boundary has been created at the bottom of the model—where the acceleration history is applied to the model (prescribed displacement)—so that no energy dissipation occurs when the acceleration history is applied to the model. The dynamic boundary conditions at the bottom boundary will let the waves pass through such that waves will not be reflected and trapped in the model.

Contact interfaces between different materials (i.e., soil and facing concrete, soil and grouted nails) have been simulated using interface elements. To do so, the shear strength reduction coefficient (R_{inter}), which is equal to the ratio of friction coefficient of two types of materials in contact with one another, has been used in the numerical model (Potyondy 1961). The soil–nail friction coefficient values were determined using laboratory interface shear tests and pullout tests on a cement-grouted nail and the surrounding soil. The results showed that the ratio of nail interface friction angle over soil friction angle is in a range of 0.67–1.05. An approximate value of 0.73 is considered reasonable for the interface strength reduction

Fig. 4 The geometry and specifications of the developed finite element model

factor in the current study. For modeling the soil-concrete and soil–nail interactions, the interface strength reduction factors of 0.65 and 0.73 were considered in the numerical simulation, respectively.

A proper mesh was created based on the concept of an adequate number of elements fitting within the wavelength of a shear wave. This shear wave was calculated as the ratio of the lowest shear wave velocity, and the highest frequency desired to be resolved to obtain a maximum characteristic dimension of the elements, always satisfying the well-known condition by Kuhlmeier and Lysmer (1973) (Eq. 14):

$$\Delta l < \frac{\lambda_{\min}}{10} = \frac{V_{s_{\min}}}{10f_{\max}}, \tag{13}$$

where $V_{s_{\min}}$ is the lower shear wave velocity of the system, f_{\max} the maximum frequency component of the input motion and Δl is the maximum spacing of the Finite Element nodes.

The procedure of simulating the excavation in the finite element software is as follows: first, a surcharge of 30 kN/m² generated by the three-story building adjacent to the trench wall is considered (each floor’s live + dead load = 10 kN/m²). Next, the initial displacements due to the in situ stresses in the soil are considered zero. Then, the 10 m trench wall is excavated in five steps, each consisting of a 2 m excavation, nail installation, and performing the shotcrete facing. By the completion of the trench wall simulation, seismic analysis of the model with regard to earthquake loading in the form of acceleration history is performed. The Upland earthquake acceleration history, shown in Fig. 5, with a duration of 23.43 s and maximum peak ground acceleration of 0.25 g (PGA = 0.25 g), is considered for this purpose. The amplification factor (AF) was calculated by dividing the peak horizontal ground acceleration for points located on the ground surface (points A, B, C, and D in Fig. 4) by the peak horizontal ground

acceleration of the Upland earthquake acceleration history (point E, $PGA_E = 0.25 \text{ g}$) (Eq. 14).

$$AF = \frac{PGA_{\text{surface}}}{PGA_E}. \tag{14}$$

In the last step of the numerical analysis, the safety factor will be considered. The strength reduction method (RSM) is adopted to obtain the safety factor of the models created in this study. The strength reduction method or otherwise known as the “Phi-c reduction” method, has been widely used to assess the seismic stability of soil slopes (Yang et al. 2020).

In the RSM technique, the critical failure mechanism is identified automatically, which is typically assumed in the conventional analysis. According to Dawson et al. (2000), the safety factor obtained by this technique is quite close to that calculated using conventional methods. The Plaxis platform uses a Phi-c reduction procedure, in which the strength parameters (i.e., c and φ) are reduced continually by a slight amount until reaching failure. The reduction ratio that satisfies Eq. (15) is equal to the safety coefficient.

$$K = F_R = \frac{\tan \varphi_0}{\tan \varphi_r} = \frac{c_0}{c_r}, \tag{15}$$

where F_R is the reduction ratio, φ_0 and c_0 are the initial strength parameters of soils, and φ_r and c_r are the reduced strength parameters of soils.

Results and discussion

Figure 6 presents the maximum horizontal displacements obtained from site monitoring and numerical modeling for the five stages of excavation. Monitoring the displacements of the wall has been carried out from top to bottom of the excavation using a series of reflectors and surveying instruments at definite time intervals. The field recordings were corrected by a relevant software to eliminate accidental errors. As shown in Fig. 6, there have been no large or abnormal deformations at the top or bottom of the wall during excavation. Despite the limitations in numerical modeling and the existing complexities of the soil profile, the numerical results are in relatively good agreement with those recorded in the field. After verifying the numerical results in the static condition, dynamic loading has been applied to the model to study soil amplification and dynamic response of the wall under varying soil nail conditions. The same methodology for verifying numerical models has been adopted by Tavakoli et al. (2019).

The effect of mechanical (soil–nail friction coefficient (FC), axial stiffness of the nails (AE)) and geometrical

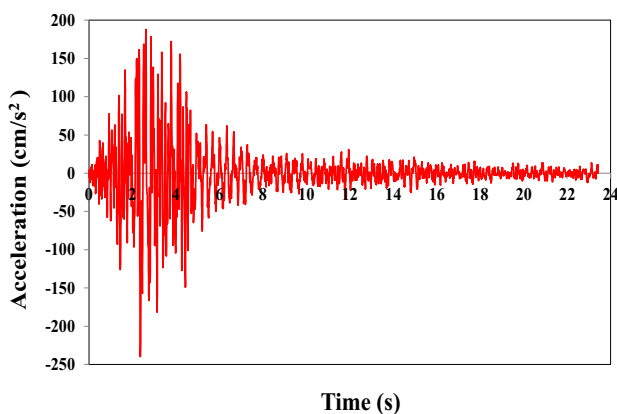


Fig. 5 The Upland earthquake acceleration history (Brinkgreve 2006)

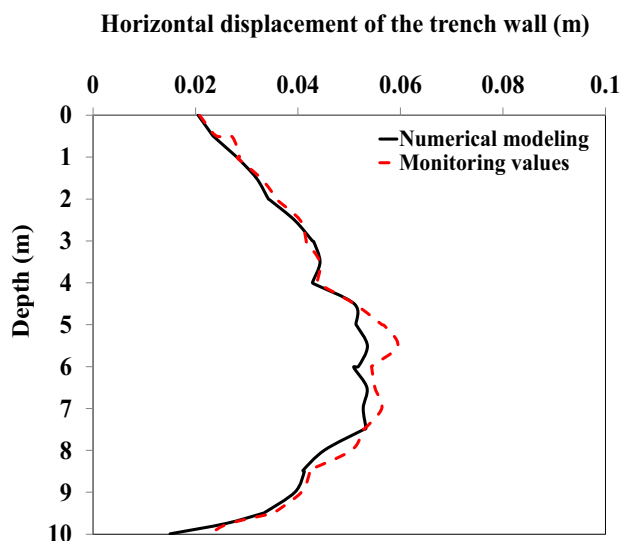


Fig. 6 Calculated and measured lateral displacement of the studied excavation

(angle (i), length (L), horizontal and vertical spacing (S_h , S_v)) parameters of the nails on the amplification factor and dynamic response of a restrained wall in loose and dense soil conditions have been investigated in a parametric manner in the following sections. The fixed and variable parameters considered in each section are presented in detail in Table 4.

Overall behavior of the soil-nailed wall under dynamic loading

In what follows, the amplification factor and dynamic response (in terms of maximum horizontal displacement, safety factor, and settlement) of the trench wall will be investigated under varying soil–nail friction coefficients, as well as nails’ axial stiffness (EA), angle, length, and spacing. The amplification factor (AF) is calculated and studied in four distinctive points located on the top of the wall, each five meters apart (points A, B, C, and D in Fig. 4).

The results of Figs. 7a, 8, 9, 10, 11 and 12a indicate that in all cases studied, the amplification factor in point A on the top of the wall is the greatest. This is primarily due to the geometry of the excavation, which concentrates the energy flow of a seismic motion on the tip of the excavation. To be clear, according to the conservation of elastic energy, energy flux must be constant during the transmission of waves, and when seismic energy enters the excavation wall from a free-field condition, the waves are concentrated at the tip of the wall (Tavakoli et al. 2019). Such topography effect amplifies the effect of the motions greatly. By moving away from the trench wall, the amplification factor and the effect of earthquake vibrations on the ground surface decrease, indicating a reduction in the topography effect by moving farther away from the excavation tip. The reduction rate, however, is not constant. Based on Figs. 7a, 8, 9, 10, 11 and 12a, one can observe that the drastic reduction in amplification factor from point A to point B has turned into a modest reduction from point C to D. It can be anticipated that by moving farther away from the point D (equal to twice the depth of the excavation), the amplification factor becomes quite close to that of free-filed condition. Another noteworthy trend in all cases studied is that the dense soil exhibited a smaller reduction in the amplification factor by moving away from the excavation tip than the loose soil, denoting that the dense ground is less influenced by the topography effect.

Moreover, it could be stated from Figs. 7a, 8, 9, 10, 11 and 12a that the amplification factor for the loose site is greater than that of the dense site in all cases studied. Amplification of earthquake effects is greatly influenced by the properties of the soil and the nature of the excitations. In general, soft grounds are notorious for amplifying the effects of earthquakes greatly; hence engineers are often quite conservative when dealing with them.

Another general behavior observed in all cases studied in the following sections is that the maximum lateral displacement and settlement of the loose soil is greater than that of the dense soil in all varying conditions of the trench wall nailing (Figs. 7b, 8, 9, 10, 11 and 12b, d). This result is in tune with the safety factor results, which is greater for

Table 4 Fixed and varied parameters in each case studied

Parametric analyses no.	Fixed parameters						Variable parameters					
	FC (–)	L (m)	S_h (m)	S_v (m)	i (Deg)	AE (kN)	FC (–)	L (m)	S_h (m)	S_v (m)	i (Deg)	AE (kN)
FC	–	7	1	1	15	2.14×10^5	0.65–1.05	–	–	–	–	–
L	0.73	–	1	1	15	2.14×10^5	–	6–9	–	–	–	–
S_h	0.73	7	–	1	15	2.14×10^5	–	–	1–2.5	–	–	–
S_v	0.73	7	1	–	15	2.14×10^5	–	–	–	1–2.5	–	–
i	0.73	7	1	1	–	2.14×10^5	–	–	–	–	10–20	–
AE	0.73	7	1	1	15	–	–	–	–	–	–	1.5×10^5 to $- 3.5 \times 10^5$

the dense soil than the loose soil in all cases studied under different nailing conditions. The relationship between the three mentioned responses is simply justified as the loose soil is in a more vulnerable stability condition, leading to greater lateral deformations and, finally, larger settlements in the adjacent ground.

The results also reveal that the maximum displacements in the lower portion of the wall under dynamic loading are greater than that in the top of the wall for both loose and dense sites in all cases studied. This is interestingly similar to the static results obtained from monitoring the actual excavation. The extent of difference between the top and bottom displacements, however, is not similar in the loose and dense sites. Based on the results of Figs. 7b, 8, 9, 10, 11 and 12b, the lateral displacement on the top of the wall is significantly less than on the bottom in the dense site.

Having discussed the general and repetitive behaviors of the modeled soil-nailed wall, the dynamic response of the wall in terms of safety factor, maximum horizontal displacement, and settlement, as well as the computed amplification factor, will be investigated parametrically considering specific conditions for the soil-nailed wall in each distinctive cases.

Effect of soil–nail interface friction

As already mentioned in Sect. “Numerical modeling”, the soil–nail interface friction coefficient is considered 0.73 in this study. To evaluate the effects of the soil-grouted nail interface friction coefficient on the amplification factor and dynamic response of the modeled trench walls, different coefficient values (0.65, 0.75, 0.85, 0.95, and 1.05) have been

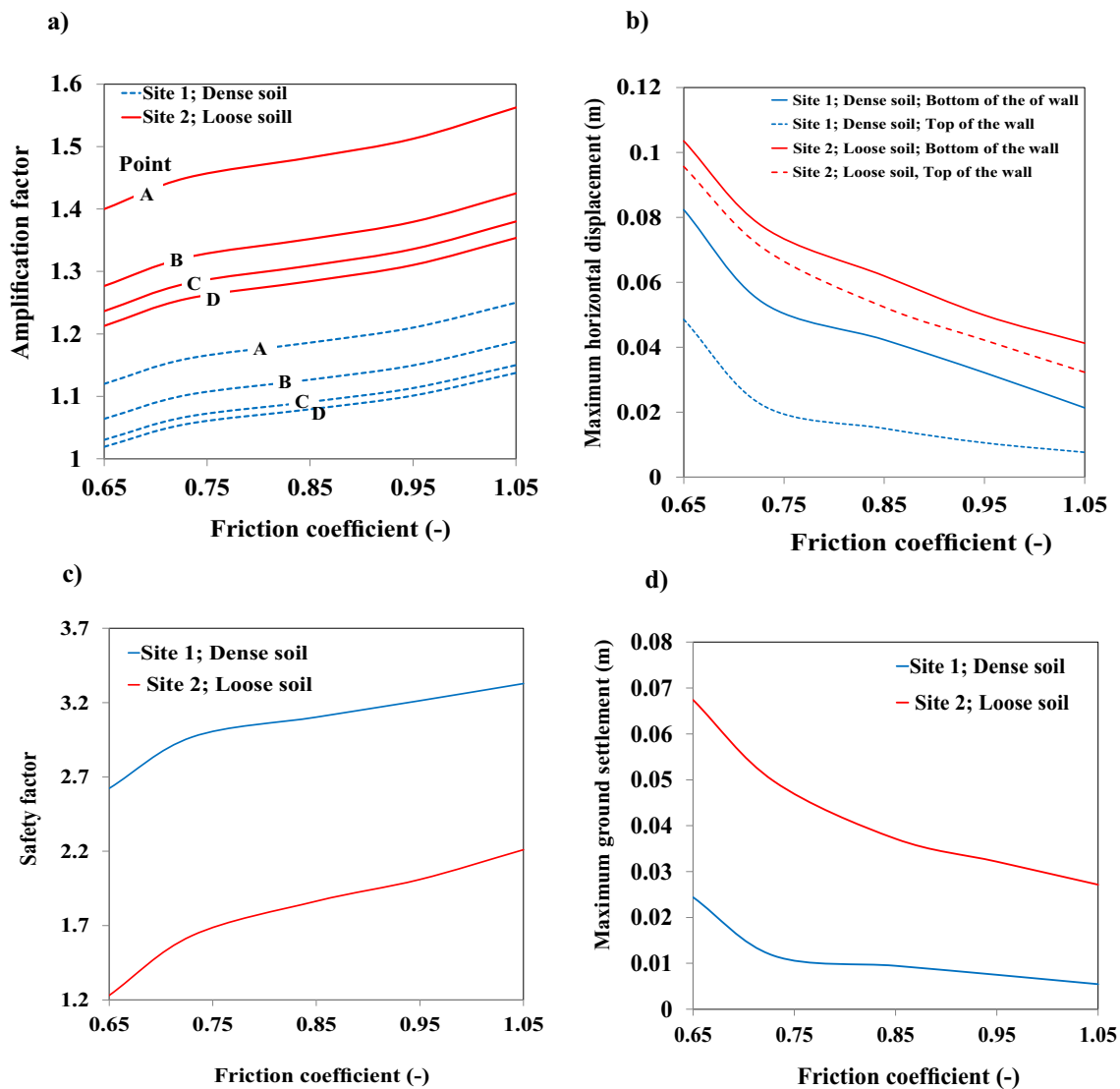


Fig. 7 Effect of the soil–nail friction coefficient on the **a** amplification factor, **b** maximum lateral displacement, **c** safety factor, and **d** maximum settlement of the trench wall

considered in the numerical modeling. The fixed parameters considered in this section can be found in Table 4.

As shown in Fig. 7a, the increase in the soil–nail friction coefficient increases the amplification factor in points A, B, C, and D (shown in Fig. 4). The increasing trend of the amplification factor fully complies with the dynamic safety factor and horizontal displacement results, which increase (Fig. 7c) and decrease (Fig. 7b), respectively, as the soil–nail friction coefficient increases. The amplification factor enlargement is mainly due to the reduction in the soil shear strains resulting from the increase in the shear strength of the failure surface provided by the employed stabilization. As a consequence, deformation of the wall decreases,

and hence energy dissipation diminishes, all leading to the increase in the amplification factor.

As stated in Sect. “Overall behavior of the soil-nailed wall under dynamic loading”, results from Fig. 7b also show that the maximum lateral displacement in the lower portion of the wall is greater than that in the top of the wall. Loose soil, of course, exhibited greater maximum lateral displacements. According to Fig. 7d, the increase in the soil–nail friction coefficient in both dense and loose soils would lead to a reduction in settlement of the adjacent ground. According to Fig. 7d, the lowest friction coefficient (friction coefficient of 0.65) in the loose site has established quite a considerable settlement (circa 7 cm)

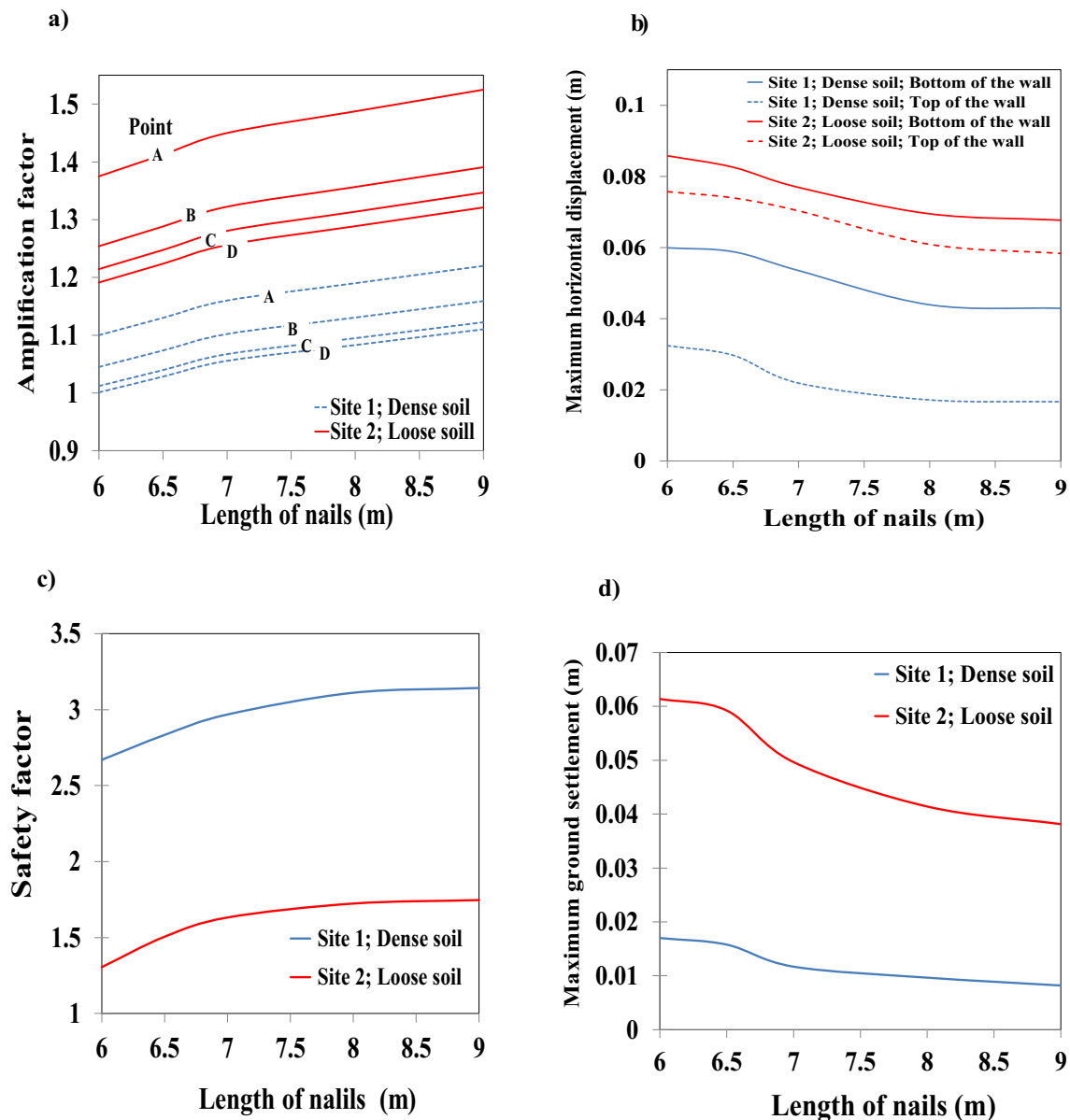


Fig. 8 Effect of the nails’ length on the **a** amplification factor, **b** maximum lateral displacement, **c** safety factor, and **d** maximum settlement of the trench wall

in the adjacent ground, which can trigger severe damages to the existing buildings. It can also be noted that the settlement of the loose site is more or less about 200 percent greater than the dense case. In the following sections, even higher levels of settlements have been obtained for the loose site with inappropriately low soil-nailed wall parameters. Therefore, proper soil–nail wall parameters should be considered to circumvent such problematic settlements in loose ground conditions under dynamic loading.

Effect of the length of the nails

According to Table 4, the dynamic response and amplification factor of the simulated model, reinforced with nails of different lengths, are evaluated in this section. As can be seen in Fig. 8, the increase in the length of the inserted

nails, in both loose and dense sites, results in an increase in the safety factor as well as a reduction in the deformations of the soil-nailed wall system. The increase in stability and decrease in the displacements leads to a reduction in the shear strains and energy dissipation of the system under dynamic loading, both of which, in turn, increase the amplification factor (Fig. 8a).

The results of Fig. 8b, c, indicating a decrease in the lateral deformations and an increase in the safety factor, respectively, can be explained by the fact that as the nails' length increases, the engagement of the failure wedge with the soil behind it increases through an increase in the friction created between the nails and the soil behind the failure wedge. This consequently enhances the wall's stability and reduces its lateral displacements. The total friction force of the nails depends on the length of the conflict zone

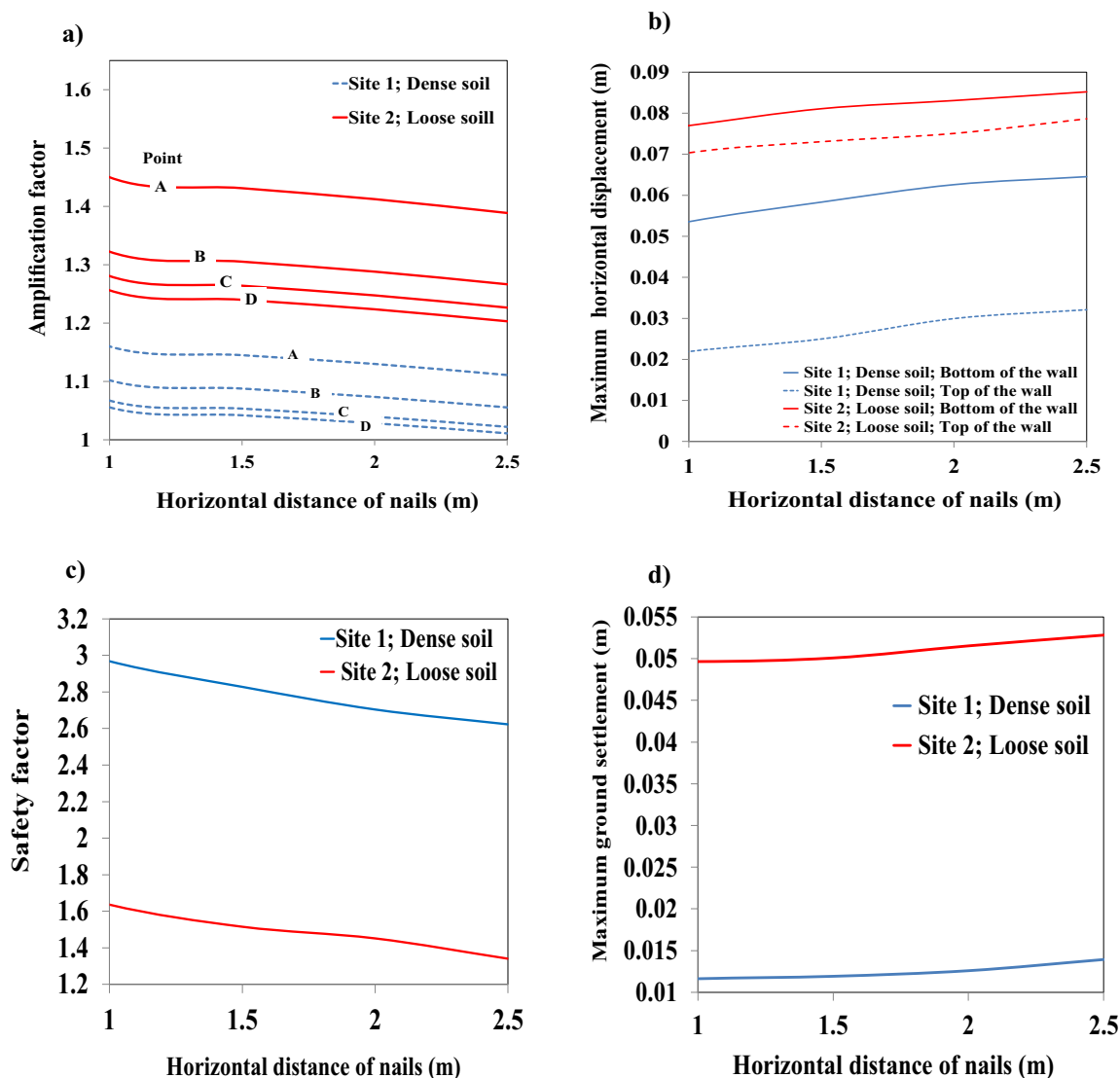


Fig. 9 Effect of the horizontal spacing of the nails on the **a** amplification factor, **b** maximum lateral displacement, **c** safety factor, and **d** maximum settlement of the trench wall

behind and in front of the failure wedge. Therefore, the increase in the length of the nails would lead to an increase in the length of the nails behind the failure wedge, and in this state, the failure wedge will be properly connected to the soil behind it. The results presented in Fig. 8 indicate that the rate of increase in the safety factor and amplification factor becomes gentler for the nails longer than 7 m. It also shows that the rate of settlement and horizontal displacement reduction drops for the nails longer than 7 m. So much so that the insertion of nails longer than 8 m is neither effective in increasing the safety factor nor controlling the horizontal displacements and ground settlements. This shows that the optimum length of the nails for the simulated wall is about 7 m, and at the length of 8 m, the

failure wedge is properly connected to the soil behind it, longer than which the length of the nails becomes inconsequential in the mentioned parameters.

Effect of the horizontal and vertical nails' spacing

Figures 9a and 10a illustrate the effect of the horizontal and vertical nails' spacing on the amplification factor of both loose and dense reinforced grounds for different locations considered in the model (Fig. 4). It is clear at first glance that both plots are almost identical in their decreasing trend as their horizontal (Fig. 9a) and vertical (Fig. 10a) nails' spacing increases. The amplification results are also perfectly in line with the results of the safety factor that show

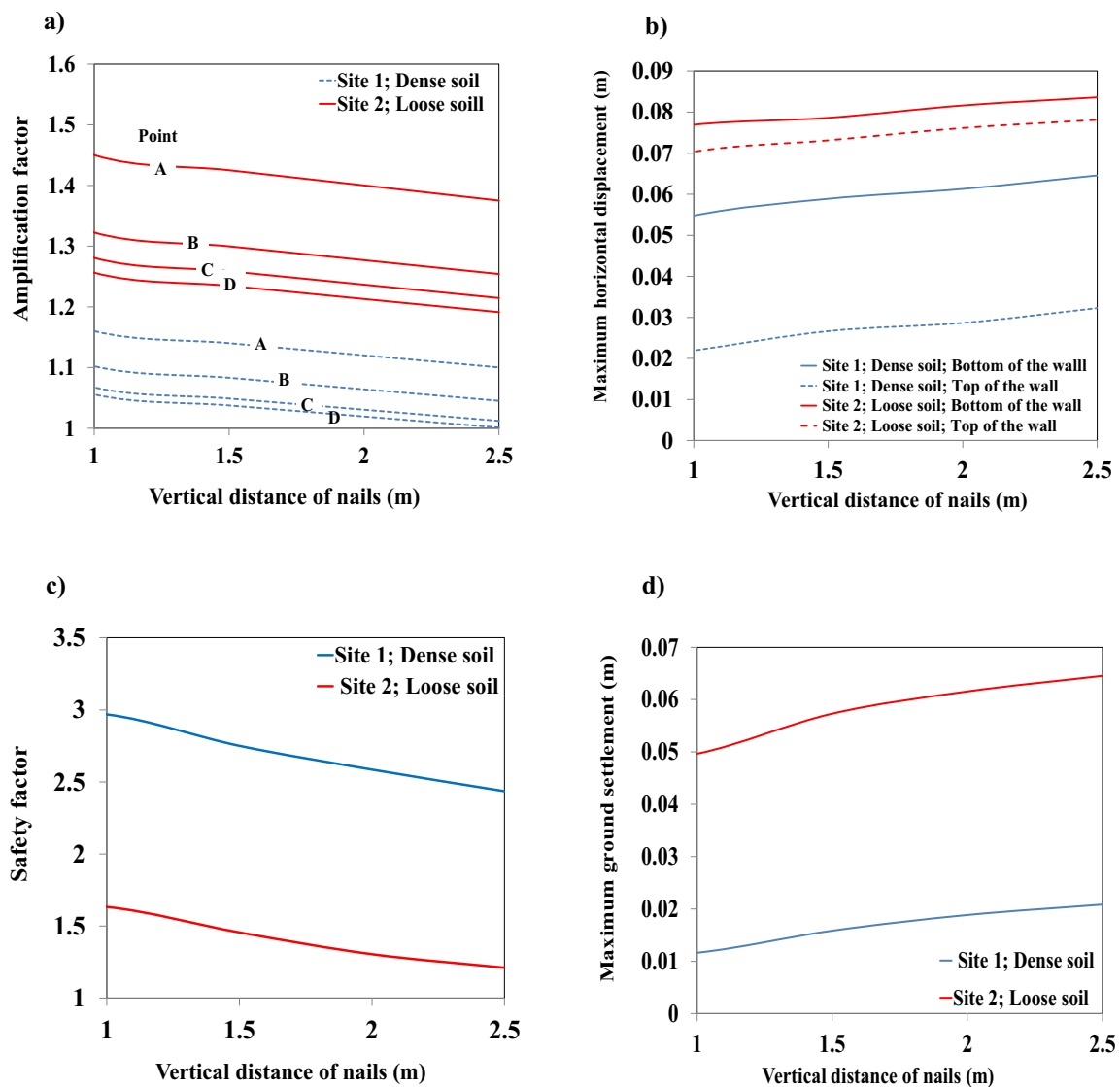


Fig. 10 Effect of the vertical spacing of the nails on the **a** amplification factor, **b** maximum lateral displacement, **c** safety factor, and **d** maximum settlement of the trench wall

a reduction as the horizontal and vertical nails' spacing increase (Figs. 9c, 10c, respectively). As previously discussed, the amplification of earthquake effects is highly influenced by the energy dissipation that occurs in the system. In this case, as the spacing of the nails becomes greater (undermining the wall's stability), larger deformations and hence shear strains would materialize, leading to the dissipation of a greater amount of energy in the system, which ultimately results in the amplification of smaller factors.

It can be observed that in both loose and dense sites, by increasing the horizontal and vertical distance of the nails from one another, the dynamic stability of the wall is compromised, and the maximum lateral displacement of the wall escalates (Figs. 9b, 10b). Similarly, the settlement results presented in Figs. 9d and 10d show an increase in settlement

of the adjacent ground as the nails' horizontal and vertical spacing increases, with the settlement of the loose ground being greater than that of the dense ground. In fact, the increase in the horizontal and vertical distance of the nails decreases the number of reinforcements inserted into the wall, which in turn, decreases the number of engagement factors that connects the failure wedge with the soil behind (decreasing the number of friction zones created between the nails and the surrounding soil) all of which ultimately lead to a decrease in total frictional forces acting behind and in front of the failure wedge.

It is worth noting that the increase in the horizontal distance of the nails is almost inconsequential in the ultimate settlement of the adjacent ground. By comparing the Figs. 9d and 10d, one can observe that while the increase

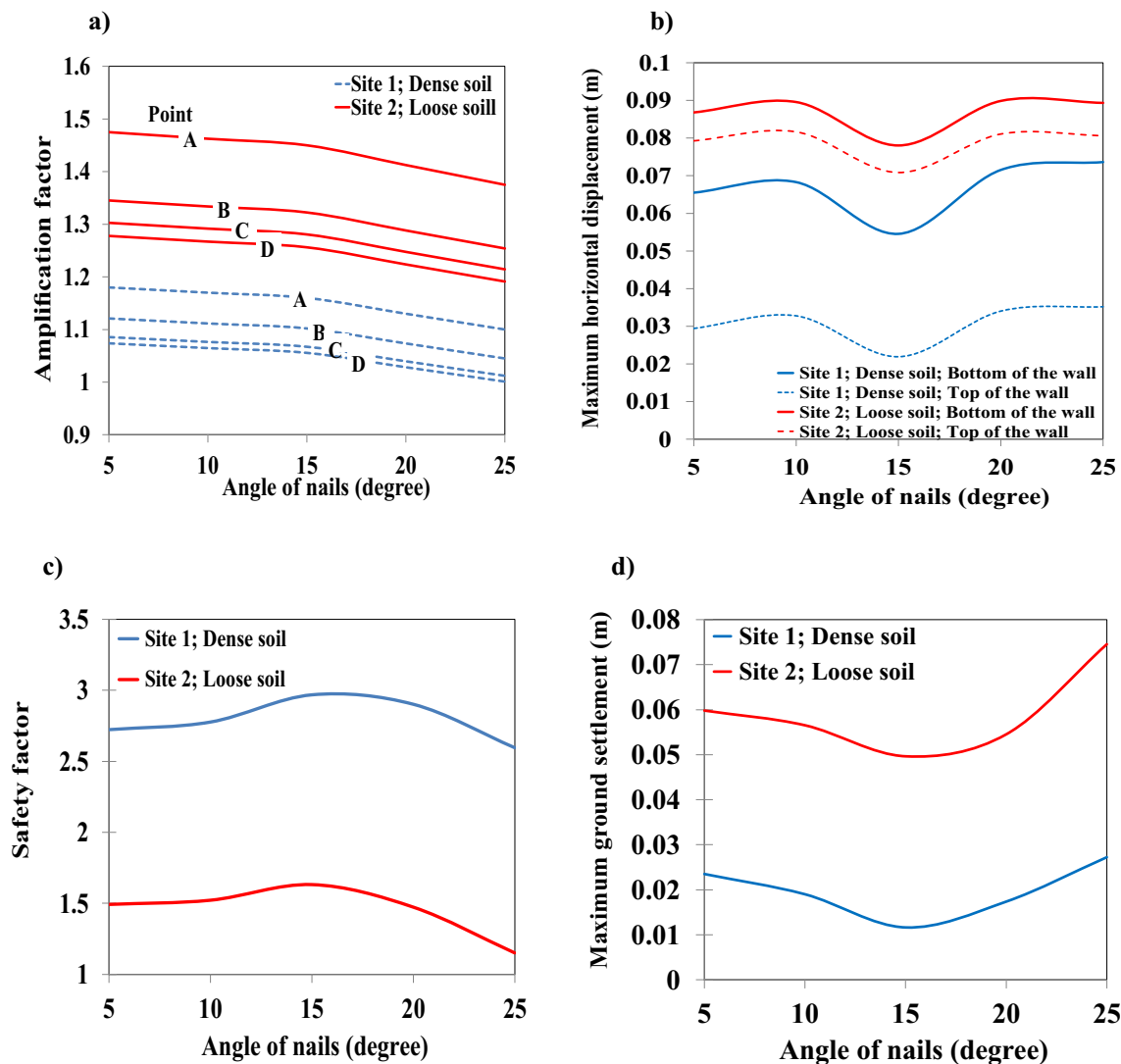


Fig. 11 Effect of the nails' inclination angle on the **a** amplification factor, **b** maximum lateral displacement, **c** safety factor, and **d** maximum settlement of the trench wall

in the vertical distance of the nails increased the settlement substantially, the increase in the horizontal nails' spacing was almost uninfluential in the settlement of the adjacent ground. The results of maximum lateral displacement and safety factor for vertical and horizontal spacing (Figs. 9b, c, 10b, c), on the other hand, exhibit no tangible difference between the effect of the horizontal and vertical spacing increase on the results. Therefore, based on the results obtained, it can be suggested that for controlling the settlement of ground in the vicinity of excavations, the reduction in the vertical spacing of the nails should be considered.

Effect of the inclination angle of the nails

The influence of nails' inclination angle on the amplification factor and dynamic response of the modeled soil-nailed wall system in both loose and dense sites has been investigated

in this section. Figure 11a shows the effect of the nailing angle on the amplification factor (AF) for points A, B, C, and D in both loose and dense grounds. It can be seen that the amplification factor results, unlike the previous sections, do not indicate significant variations. Based on Fig. 11a, the amplification factor has dropped by a modest 6.8% from the angle of 5° – 25° . The safety factor, horizontal displacement, and settlement results have also shown a minute reduction in the mentioned range, that is, a reduction of 14.8% for the safety factor, an increase of 8.5% for lateral displacement, and an increase of 20% for the settlement. It can be inferred from the mentioned results that the slight decrease in the stability and increase in deformations has yielded a modest increase in the shear strains and damping, all leading to an insignificant decrease in the amplification factor.

However, there is a discontinuity in the wall's behavior in the mentioned range. Although, in general, the stability

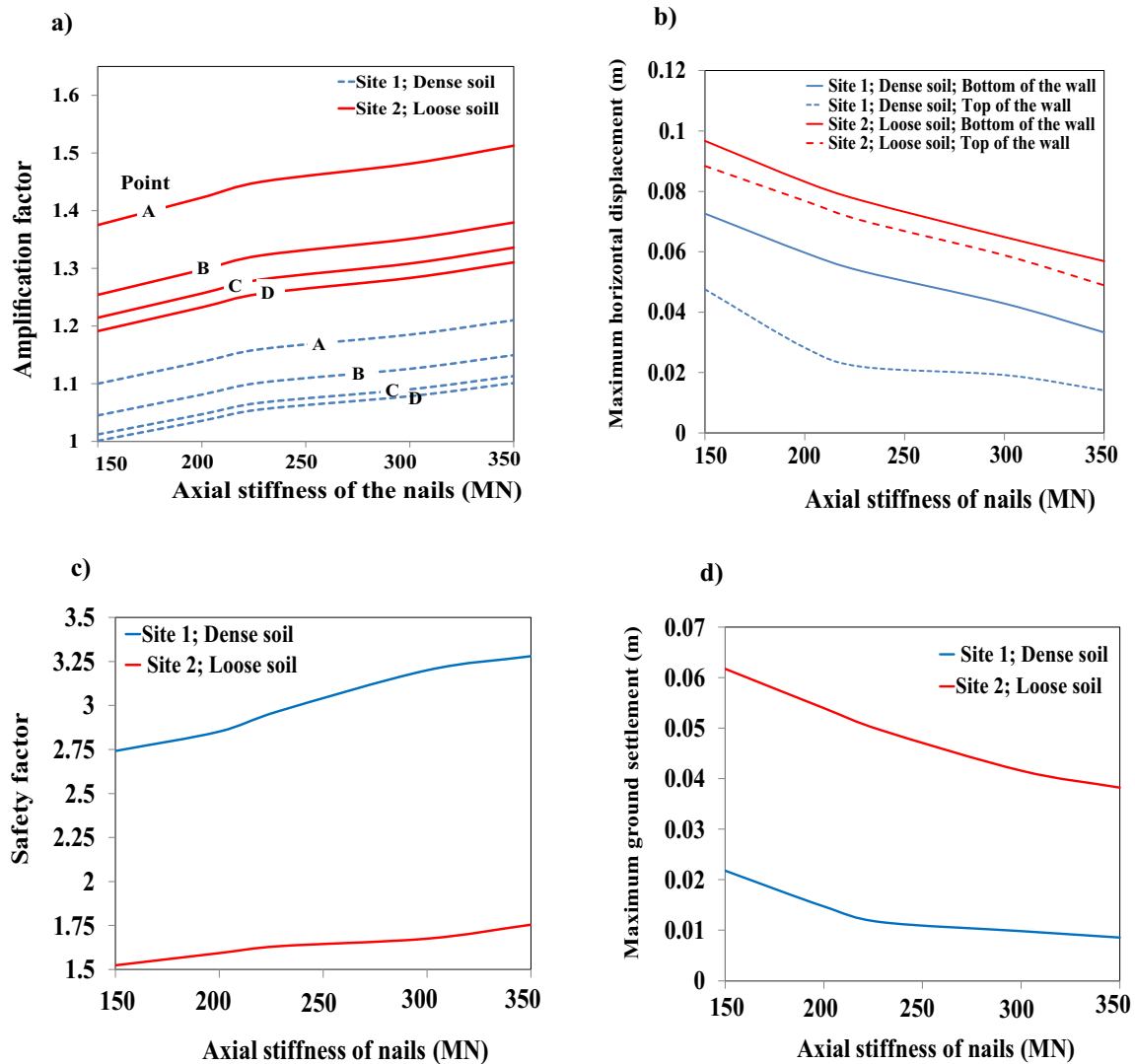


Fig. 12 Effect of the nails' axial stiffness on the **a** amplification factor, **b** maximum lateral displacement, **c** safety factor, and **d** maximum settlement of the trench wall

of the wall diminished from angle 5 to 25, the trend was not continuous as the stability increased from the nail angle of 5 to 15 and then decreased. This is due, in large part, to the fact that there is an optimum nail angle at which the performance of the modeled soil-nailed wall in terms of dynamic stability and displacement is the best. Therefore, there is no definite increasing or decreasing trend in the shear strains and damping of the system that would result in a considerable and continuous variation in the amplification factor of the simulated model. It could be said that, at this specific turning point (angle of 15°), the installed nails have properly connected the failure wedge to the soil behind it. The same behavior has also been observed in the work of (Maleki and Mir Hosseini 2022).

The determination of an appropriate nailing angle becomes specifically important when working on very narrow margins in terms of the safety factor. For instance, according to Fig. 11c, it could be noted that for nailing angles of greater than 18° in the loose site, the safety factor of the wall could fall well below the permissible range proposed by the code (minimum safety factor for global stability of excavation is $F.S_G = 1.35$, FHWA code 2017). The optimum nailing angle in the mentioned model, on the other hand, would offer an acceptable safety factor greater than 1.5.

Effect of the axial stiffness of the nails (EA)

In this section, the influence of the axial stiffness of the nails on the amplification factor and dynamic response of both sites modeled will be investigated. The fixed and variable parameters considered herein are presented in detail in Table 4.

The result of the amplification factor under varying nails' axial stiffness is presented in Fig. 12a for points considered on top of the wall for both loose and dense sites. In line with the safety factor results, which show an increase as the axial stiffness of the nails increases (Fig. 12c), the amplification factor also increases as the axial stiffness of the nails increases. The substantial limitation in the lateral displacement of the wall and the settlement of the adjacent ground (Fig. 12b, d) is the reason behind this behavior, as the drop in the mentioned deformations would directly result in a drop in the shear strains and energy dissipation in the system and hence the amplification factor enlarges. Dynamic response of the wall in terms of the maximum horizontal displacements, safety factor, and maximum settlement of the adjacent ground are presented in Fig. 12b–d, respectively. The results demonstrate that the increase in the axial stiffness of the nails would yield a considerable increase in the safety factor and controls the lateral displacements and settlement of the system up to a great extent. The stability enhancement and displacement control are achieved owing

to the increase in the tensile forces acting against the total active forces of the reinforced wall.

Economic evaluation

Economics is a very important component of civil engineering. In order for a project to be successful, it must be affordable and return more value than it costs. Without a firm understanding of costs, one cannot properly evaluate the feasibility and cost-effectiveness of any project. Therefore, the study is supplemented with a short discussion on the influence of each of the mentioned parameters on the economy of a typical trench wall stabilization project. The positive impact of some of the parameters studied thus far is achieved at the expense of either the use of a greater amount of resources or the use of materials with superior quality. For instance, installation of longer nails or insertion of a larger number of nails due to a reduction in the nails' spacing would, of course, enhance the performance but requires the use of more materials. The insertion of nails with higher axial stiffness, on the other hand, would require the use of materials with higher quality. All of the mentioned measures can jeopardize the economy of a project and put an extra burden on the environment due to the production of such materials. Nevertheless, through a smart design, such financial and environmental burdens can be averted without compromising the dynamic performance of a trench wall or slope. As discussed in Sect. “[Effect of the inclination angle of the nails](#)”, the insertion of nails at an optimum angle would certainly not be an expensive undertaking, yet it can improve the response in terms of stability, lateral displacement, and settlement by an astonishing 9.2%, 15%, and 34% on average for both loose and dense sites. In addition, through the use of proper adhesives, compliant with the nails and the specific type of soil being reinforced, the friction coefficient of both interacting materials can be improved substantially, which in turn, results in the improvement of the response by a great deal; in our case, for instance, the increase of 23% in the safety factor and the reduction of 34% and 40% in the lateral displacements and settlement, respectively, can be achieved by a mere 12% increase in the soil–nail friction coefficient.

Conclusions

The influential parameters in dynamic response and amplification of an excavation restrained by a nailing system have been studied numerically. The investigation has been carried out by considering varying soil–nail conditions for

the developed model. Such conditions include the mechanical (soil–nail friction coefficient and nail’s axial stiffness) and geometrical (angle, length, and spacing) properties of the nails installed in both loose and dense soils. The major findings of the present research are summarized in the following paragraphs.

It was observed that the factors leading to an increase in the stability and a decrease in the deformation of the wall would also lead to an increase in the amplification factor. This is due, in large part, to the fact that the increase in the stability causes a decrease in the wall’s tendency to exhibit greater nonlinear behavior through larger deformations, which in turn, results in the generation of smaller shear strains and dissipation of a smaller amount of energy in the created model. Based on the results obtained, the increase in the nails’ length, axial stiffness, and the soil–nail friction coefficient result in an increase in the stability and a decrease in the deformations under dynamic loading, all leading to an increase in the amplification factor of the trench wall. Conversely, the increase in the nails’ spacing would result in a decrease and increase in the wall’s stability and deformations, respectively, both increasing the nonlinear behavior, shear strains, and energy dissipation in the reinforced system, all contributing to the amplification factor reduction. As for the nails’ angle of insertion, there is no continuous decreasing or increasing trend in the stability or deformation of the trench wall. There is, however, a turning point at the nailing angle of 15° at which the highest stability and the least deformation have been computed in the model.

The results also revealed that the highest amplification factor is expected in the immediate vicinity of the trench wall as a result of the topography effect and the concentration of the seismic waves at the tip of the excavation. By moving away from the tip of the wall, the amplification factor decreases, indicating a reduction in the topography effect. In addition, the reduction rate decreases by moving farther away from the tip of the excavation, so much so that, at a distance of twice the excavation depth, the amplification factor becomes quite close to that of the free-field condition. The dense soil, compared to the loose soil, exhibited a smaller reduction in the amplification factor by moving away from the excavation tip. The presented results emphasize that special considerations should be taken into account for structures constructed in the vicinity of a reinforced excavation in the light of such site effects as amplification factor and topography effects.

Based on the results obtained, the effect of nails’ length on the performance of the wall wears off for nails longer than 8 m. Moreover, the amplification factor reduction rate drastically decreased for the vertical and horizontal nails’ spacing of more than 1 m. There is also an optimum nailing

angle at which the response of the wall is the most desirable. It was also noted that the vertical spacing of the nails is more influential in the control of the settlement of the adjacent ground compared to the horizontal spacing.

The results also showed that, as expected, the loose site amplified the earthquake effects by a larger factor than the dense soil. It also exhibited inferior dynamic response in terms of safety factor and deformations compared to the dense site in all varying nailing conditions. The results also revealed that, similar to the monitoring results recorded under static loading, the displacements in the lower portion of the wall under dynamic loading are greater than that in the top of the wall for both loose soil and dense sites in all cases studied.

Funding No type of funding has been used to support this study.

Data availability Available per request.

Declarations

Conflict of interest The authors declare that they have no conflict of interest.

References

- Committee ACI (1995) Building code requirements for structure concrete and commentary. American Concrete Institute, Farmington Hills
- Atkinson JH, Sallfors G (1991) Experimental determination of soil properties. In: Proceedings of 10th ECSMFE, Florence 3, pp 915–956
- Bang SC, Chung YI (1999) The effect of the nail skew angle of soil nailing wall. *KSCE J Civ Eng* 3:73–79. <https://doi.org/10.1007/BF02830737>
- Benz T (2007) Small-strain stiffness soft soil and its numerical consequences. Ph.D. thesis, Univ. of Stuttgart, Stuttgart, Germany
- Bolton MD (1986) The strength and dilatancy of sands. *Geotech J Geotech Eng* 36:65–78. <https://doi.org/10.1680/geot.1986.36.1.65>
- Brinkgreve RBJ (2012) Plaxis 3D material models manual. Delft University of Technology and Plaxis bv, Delft
- Brinkgreve RBJ, Broere W, Waterman D (2006) Plaxis, finite element code for soil and rock analyses users manual, The Netherlands
- Chavan D, Mondal G, Prashant M (2017) Seismic analysis of nailed soil slope considering interface effects. *Soil Dyn Earthq Eng* 100:480–491. <https://doi.org/10.1016/j.soildyn.2017.06.024>
- Chatterjee K (2022) Influence of surcharge loading on seismic response of nailed soil slopes. *Geo-Congress 2022 (ASCE)*. Charlotte, North Carolina. <https://doi.org/10.1061/9780784484029.046>
- Chen GH, Zou JF, Yang T et al (2022) Three-dimensional modified pseudo-dynamic analysis of reinforced slopes with inclined soil nails. *Bull Eng Geol Environ* 81:377. <https://doi.org/10.1007/s10064-022-02886-7>
- Clough RW, Penzien J (1993) Dynamics of structures, vol 634. McGraw-Hill, New York

- Colin JG, Chouery-Curtis VE, Berg RR (1992) Field observations of reinforced soil structures under seismic loading. In: Proceedings of the international symposium on earth reinforcement. Fukuoka, Japan, vol 1, pp 223–228
- Dawson EM, Roth WH, Drescher A (2000) Slope stability analysis by strength reduction. *Geotechnique* 49(6):835–840. <https://doi.org/10.1680/geot.1999.49.6.835>
- Debabrata G, Aniruddha S (2010) Dynamic behavior of small-scale model of nailed steep slope. *Geomech Geoeng* 5:99–108. <https://doi.org/10.1080/17486020903497415>
- Deng D, Li L, Zhao Lh (2017) Limit equilibrium analysis for stability of soil nailed slope and optimum design of soil nailing parameters. *J Cent South Univ* 24:2496–2503. <https://doi.org/10.1007/s11771-017-3662-y>
- Duncan JM, Chang CY (1970) Nonlinear analysis of stress and strain in soils. *J Soil Mech Found Div ASCE* 96:1629–1653
- Fakher A, Cheshomi A, Khamechiyan M (2007) The addition of geotechnical properties to a geological classification of coarse-grained alluvium in apediment zone. *Q J Eng GeolHydrogeol* 40(2):163–174. <https://doi.org/10.1144/1470-9236/06-029>
- Fan CC, Luo JH (2008) Numerical study on the optimum layout of soil nailed slopes. *Comput Geotech* 35(4):585–599. <https://doi.org/10.1016/j.compgeo.2007.09.002>
- Farrokhzad F, Motahari Tabari S, Abdolghafoor kashani H (2017) Seismic behaviour of excavations reinforced with soil-nailing method. *Geotech Geol Eng* 39:4071–4091. <https://doi.org/10.1007/s10706-020-01625-7>
- FHWA0-IF-03-017 (2017) Federal Highway Administration, U.S. Department of Transportation, Washington DC, USA
- Giri D, Sengupta A (2009) A kinematic limit approach for the stability analysis of nailed soil slopes. *Asian J Civ Eng (build Hous)* 10(2):163–176
- He S, Ouyang C, Luo Y (2012) Seismic stability analysis of soil nail reinforced slope using kinematic approach of limit analysis. *Environ Earth Sci* 66(1):319–326. <https://doi.org/10.1007/s12665-011-1241-3>
- Jaky J (1994) The coefficient of earth pressure at rest. *J Soc Hungar Arch Eng* 8(22):355–358
- Jaya V, Annie J (2013) An investigation on the dynamic behavior of soil nail walls. *J Civ Eng Sci* 2(4):241–249
- Johari A, Hajivand AK, Binesh S (2020) System reliability analysis of soil nail wall using random finite element method. *Bull Eng Geol Environ* 79:2777–2798. <https://doi.org/10.1007/s10064-020-01740-y>
- Khoiri M, Ou CY (2013) Evaluation of deformation parameter for deep excavation in sand through case studies. *Comput Geotech* 47:57–67. <https://doi.org/10.1016/j.compgeo.2012.06.009>
- Knill JL, Jones KS (1968) Ground-water conditions in Greater Tehran. *Q J Eng Geol Hydrogeol* 1(3):181–194. <https://doi.org/10.1144/gsl.qjeg.1968.001.03>
- Kramer SL (1996) Geotechnical earthquake engineering. Prentice-Hall Inc, Upper Saddle River
- Kuhlmeyer RL, Lysmer J (1973) Finite element method accuracy for wave propagation problems. *J Soil Mech Found Div* 99:421–427. <https://doi.org/10.1061/JSFEAQ.0001885>
- Kurtulus A, Stokoe KH (2008) In situ measurement of nonlinear shear modulus of silty soil. *J Geotech Geoenviron Eng* 134:10. [https://doi.org/10.1061/\(ASCE\)1090-0241\(2008\)134:10\(1531\)](https://doi.org/10.1061/(ASCE)1090-0241(2008)134:10(1531))
- Lees A (2007) Geotechnical finite element analysis. ICE Publishing, London
- Maleki M, Mir Mohammad Hosseini S (2022) Assessment of the Pseudo-static seismic behavior in the soil nail walls using numerical analysis. *Innov Infrastruct Solut.* <https://doi.org/10.1007/s41062-022-00861-5>
- Mark RT, Mladen V (2000) Dynamic failure mechanism of soil-nailed excavation models in centrifuge. *Geotech Geoenviron Eng* 126:3. [https://doi.org/10.1061/\(ASCE\)1090-0241\(2000\)126:3\(227\)](https://doi.org/10.1061/(ASCE)1090-0241(2000)126:3(227))
- Michalowski RL, You L (2000) Displacements of reinforced slopes subjected to seismic loads. *J Geotech Geoenviron Eng* 126(8):685–694. [https://doi.org/10.1061/\(ASCE\)1090-0241\(2000\)126:8\(685\)](https://doi.org/10.1061/(ASCE)1090-0241(2000)126:8(685))
- Moniuddin MK, Manjularani P, Govindaraju L (2016) Seismic analysis of soil nail performance in deep excavation. *Int J Geo-Eng* 7:16. <https://doi.org/10.1186/s40703-016-0030-y>
- Peng FL et al (2011) Field measurements and finite-element method simulation of a tunnel shaft constructed by pneumatic caisson method in shanghai soft ground. *J Geotech Geoenviron Eng* 137:516–524. [https://doi.org/10.1061/\(ASCE\)GT.1943-5606.0000460](https://doi.org/10.1061/(ASCE)GT.1943-5606.0000460)
- Plaxis D (2017) Reference manual. Delft, Netherlands
- Potyondy JG (1961) Skin friction between various soils and construction materials. *Geotech J Geotech Eng Geotech* 11:339–353. <https://doi.org/10.1680/geot.1961.11.4.339>
- Rampello S, Viggiani G, Amorost A (1997) Small-strain stiffness of reconstituted clay compressed along constant triaxial effective stress ratio path. *Géotechnique* 47(3):475–489. <https://doi.org/10.1680/geot.1997.47.3.475>
- Rawat S, Gupta AK (2016) Analysis of a nailed soil slope using limit equilibrium and finite element methods. *Int J Geosynth Ground Eng.* <https://doi.org/10.1007/s40891-016-0076-05>
- Sahoo S, Manna B, Sharma KG (2015) Stability analysis of steep nailed slopes under seismic condition using 3-D finite element-method. *Int J Geotech Eng* 9(5):536–540. <https://doi.org/10.1179/1939787914Y.0000000084>
- Schanz T, Vermeer PA, Bonnier PG (1999) The hardening soil model: formulation and verification, beyond 2000 in computational geotechnics. Balkema, Rotterdam
- Sharma M, Choudhury D, Samanta M, Sarkar S, Annapareddy VSR (2020) Analysis of helical soil-nailed walls under static and seismic conditions. *Can Geotech J* 57(6):785–800. <https://doi.org/10.1139/cgj-2019-0240>
- Singh VP, Sivakumar Babu GL (2010) 2D numerical simulations of soil nail walls. *Geotech Geol Eng* 28(4):299–309. <https://doi.org/10.1007/s10706-009-9292-x>
- Siva Kumar Babu GL, Murthy BRS (2002) Analysis of construction factors influencing the behavior of soil nailed earth retaining walls. *Ground Improv* 6(3):137–143. <https://doi.org/10.1680/grim.2002.6.3.137>
- Siva Kumar Babu GL et al (2008) Numerical analysis of performance of soil nail walls in seismic conditions. *ISET J Earthq Technol* 45:31–40
- Tatsuoka F, Tateyama M, Koseki J, Uchimura T (1995) Geotextile-reinforced soil retaining wall and their seismic behaviour. In: Proceedings of 10th Asian regional conference on soil mechanics and foundation engineering 2, pp 26–49
- Tavakoli H, Kutanaei SS, Hosseini SH (2019) Assessment of seismic amplification factor of excavation with support system. *Earthq Eng Eng Vib* 18:555–566. <https://doi.org/10.1007/s11803-019-0521-x>
- Viggiani G, Atkinson JH (1995) Stiffness of fine-grained soil at very small strains. *Géotechnique* 45(2):249–265. <https://doi.org/10.1680/geot.1995.45.2.249>
- Wei WB, Cheng YM (2010) Soil nailed slope by strength reduction and limit equilibrium methods. *Comput Geotech* 37(5):602–618. <https://doi.org/10.1016/j.compgeo.2010.03.008>
- Wu JC, Shi R (2010) Seismic analysis of soil nailed wall using finite element method. *Adv Mater Res.* <https://doi.org/10.4028/www.scientific.net/AMR.535-537.2027>

- Yang T, Zou J, Pan Q (2020) Three-dimensional seismic stability of slopes reinforced by soil nails. *Comput Geotech* 127:103768. <https://doi.org/10.1016/j.compgeo.2020.103768>
- Yazdandoust M (2017) Experimental study on seismic response of soil-nailed walls with permanent facing. *Soil Dyn Earthq Eng* 98:101–119. <https://doi.org/10.1016/j.soildyn.2017.04.009>

Springer Nature or its licensor holds exclusive rights to this article under a publishing agreement with the author(s) or other rightsholder(s); author self-archiving of the accepted manuscript version of this article is solely governed by the terms of such publishing agreement and applicable law.

Publisher's Note Springer Nature remains neutral with regard to jurisdictional claims in published maps and institutional affiliations.